

Article

SNARE Protein AoSec22 Orchestrates Mycelial Growth, Vacuole Assembly, Trap Formation, Stress Response, and Secondary Metabolism in *Arthrobotrys oligospora*

Yingmei Zhu ¹, Duanxu Zhou ², Na Bai ¹, Qianqian Liu ¹, Na Zhao ¹ and Jinkui Yang ^{1,*} 

¹ State Key Laboratory for Conservation and Utilization of Bio-Resources in Yunnan, Key Laboratory for Southwest Microbial Diversity of the Ministry of Education, School of Life Science, Yunnan University, Kunming 650032, China

² College of Forestry and Biotechnology, Zhejiang A&F University, Hangzhou 311300, China

* Correspondence: jinkui960@ynu.edu.cn

Abstract: Soluble N-ethylmaleimide-sensitive factor attachment protein receptors (SNAREs) facilitate intracellular vesicle trafficking and membrane fusion in eukaryotes and play a vital role in fungal growth, development, and pathogenicity. However, the functions of SNAREs are still largely unknown in nematode-trapping fungi. *Arthrobotrys oligospora* is a representative species of nematode-trapping fungi that can produce adhesive networks (traps) for nematode predation. In this study, we characterized AoSec22 in *A. oligospora*, a homolog of the yeast SNARE protein Sec22. Deletion of *Aosec22* resulted in remarkable reductions in mycelial growth, the number of nuclei, conidia yield, and trap formation, especially for traps that failed to develop mature three-dimensional networks. Further, absence of *Aosec22* impaired fatty acid utilization, autophagy, and stress tolerance; in addition, the vacuoles became small and fragmented in the hyphal cells of the $\Delta Aosec22$ mutant, and large vacuoles failed to form. The reduced sporulation capacity correlated with the transcriptional repression of several sporulation-related genes, and the impaired accumulation of lipid droplets is in line with the transcriptional repression of several genes involved in fatty acid oxidation. Moreover, absence of *Aosec22* remarkably impaired secondary metabolism, resulting in 4717 and 1230 compounds upregulated and downregulated in the $\Delta Aosec22$ mutant, respectively. Collectively, our data highlighted that the SNARE protein AoSec22 plays a pleiotropic role in mycelial growth and development, vacuole assembly, lipid metabolism, stress response, and secondary metabolism; in particular, it is required for the proper development of traps in *A. oligospora*.

Keywords: *Arthrobotrys oligospora*; SNARE protein; conidiation; vacuole assembly; trap formation; secondary metabolism



Citation: Zhu, Y.; Zhou, D.; Bai, N.; Liu, Q.; Zhao, N.; Yang, J. SNARE Protein AoSec22 Orchestrates Mycelial Growth, Vacuole Assembly, Trap Formation, Stress Response, and Secondary Metabolism in *Arthrobotrys oligospora*. *J. Fungi* **2023**, *9*, 75. <https://doi.org/10.3390/jof9010075>

Academic Editor: Ming-Guang Feng

Received: 16 December 2022

Revised: 31 December 2022

Accepted: 31 December 2022

Published: 4 January 2023



Copyright: © 2023 by the authors. Licensee MDPI, Basel, Switzerland. This article is an open access article distributed under the terms and conditions of the Creative Commons Attribution (CC BY) license (<https://creativecommons.org/licenses/by/4.0/>).

1. Introduction

Most of secreted proteins enter the endoplasmic reticulum (ER) lumen in eukaryotes [1]. The ER is the largest organelle in cells and plays a critical role in many cellular processes, including protein synthesis, trafficking of proteins, lipid synthesis, autophagy, cellular metabolism, calcium homeostasis, and detoxification [2–5]. Protein transport involves the budding and fusion of membrane vesicles between adjacent compartments, leading to the entry of the cargo into transport vesicles [6]. The fusion of vesicles with the target compartment depends on the cooperation between several conserved proteins, including small GTPases and soluble N-ethylmaleimide-sensitive factor attachment protein receptors (SNAREs) [7,8]. SNAREs play a vital role in the fusion of biological membranes and share a conserved region of 60–70 amino acid residues in plants, animals, and microorganisms, which is called the SNARE domain and is arranged in heptad repeats [9,10]. SNAREs fall into two categories: v-SNAREs in transport vesicles and t-SNAREs in target membranes [11]. v-SNAREs are located in the membranes of vesicles and t-SNAREs are present

on target membranes where they assemble into a trans-SNARE complex, forming a fitted connection between two membranes and helping in the mixing of lipid bilayers, thus allowing membrane fusion [12,13]. SNAREs are reclassified as R-SNAREs (arginine-containing SNAREs) and Q-SNAREs (glutamine-containing SNAREs) based on their conserved domain [14]. SNAREs are a large family of proteins; one R-SNARE interacts with three Q-SNAREs, named after their interacting residues arginine (R) or glutamine (Q), when they transport cargoes [15,16].

Sec22 is an R-SNARE protein that plays diverse roles in eukaryotes [17]. Sec22 localizes in the ER and Golgi and helps in anterograde and retrograde transport [18,19]. Sec22 takes part in vacuole function in both yeast and plants [20]. A loss of *sec22* in plants results in Golgi fragmentation and defects in gametophyte development [21]. In addition, Sec22 family proteins are highly conserved from yeasts to humans. Several *sec22* genes, *sec22A*, *sec22B*, and *sec22C*, were also found in humans. In cultured mammalian cells, Sec22 proteins are also required for ER to Golgi trafficking [22,23]. Recently, the R-SNARE homolog Sec22 has been identified in several plant pathogenic fungi. For example, Sec22 is required for conidiogenesis, cell wall integrity, and host plant infection in *Magnaporthe oryzae* [24]. In *Fusarium graminearum*, the R-SNARE protein FgSec22 and the Q-SNARE protein FgSyn8 function similarly in hyphal growth, conidiation, deoxynivalenol (DON) production, and pathogenicity [13,25]. Deletion of the *sec22* homolog *Vdsec22* in *Verticillium dahliae* resulted in reduced virulence and perturbed secretion of the extracellular proteins involved in carbohydrate hydrolysis [26]. All of these studies demonstrated that Sec22 was a key regulator of the secretory pathway.

Nematode-trapping (NT) fungi are a group of filamentous species that can produce special mycelial traps to capture and digest nematodes in all ecosystems worldwide [27,28]. *Arthrobotryx oligospora* is a typical NT fungus, widely spread in diverse environments, and hence a model to study interactions between fungi and nematodes [29]. *A. oligospora* produces adhesive networks when stimulated in the presence of nematodes or other inducing factors, indicating a switch from the saprophytic lifestyle to the predacious stage [29,30]. In *A. oligospora*, several signaling proteins involved in the regulation of trap formation and pathogenicity have been identified, including mitogen-activated protein kinase (MAPK) [31], G protein β subunit [32], regulators of G protein signaling [33,34], and small GTPases Rab-7A [35], Ras [36], and the Rho family [37]. Recently, a homolog of the yeast SNARE protein Vam7 was revealed to play an important role in vegetative growth, conidiation, trap formation, and ring cell inflation in the constricting ring-forming NT fungus *Drechlerella dactyloides* [38]. However, the functions of SNAREs are still largely unknown in the lifecycle of *A. oligospora*.

This study sought to characterize AoSec22, homologous to the yeast SNARE protein Sec22 in *A. oligospora*, by multiple analyses of targeted gene disruption mutants. Deletion of the *Aosec22* gene results in decreases in vegetative growth, the number of nuclei, the conidia yield, and trap formation; in particular, the deletion mutant ($\Delta Aosec22$) failed to develop mature traps. Meanwhile, AoSec22 plays a significant role in resistance to diverse chemical stressors. In addition, AoSec22 contributes to the morphology of lipid droplets, autophagy, and vacuole assembly, and mediates secondary metabolism.

2. Materials and Methods

2.1. Strains and Culture Conditions

The wild-type (WT) fungus *A. oligospora* (ATCC24927), purchased from the American Type Culture Collection (ATCC), and the mutant strains constructed in this study were cultured on potato dextrose agar (PDA) at 28 °C in the dark. Liquid TG (1% tryptone and 1% glucose) medium was used to cultivate the fungal mycelia for DNA extraction and protoplast preparation. The *Saccharomyces cerevisiae* FY834 strain (a gift from Dr. K.A. Borkovich, University of California), used as a host to construct recombinant plasmids, was cultured in yeast-extract-peptone-dextrose medium. *Escherichia coli* DH5 α strains carrying pRS426 and pCSN44 plasmids (Tsingke, Beijing, China) were grown in Luria-Bertani broth

agar supplemented with 50 µg/mL kanamycin or 100 µg/mL ampicillin. *Caenorhabditis elegans* was incubated at 25 °C on oatmeal medium and used to induce trap formation in bioassays [39].

2.2. Bioinformatic Analysis of AoSec22

The AoSec22 (AOL_s00076g350) was identified based on the amino acid sequences of orthologous Sec22 from the model fungi *Aspergillus nidulans* and *M. oryzae*. The isoelectric point (pI) and molecular weight (MW) of AoSec22 were calculated with the pI/MW tool (http://www.expasy.ch/tools/pi_tool.html) (accessed 19 August 2022), and functional domains were predicted with the default parameters of InterProScan (accessed 19 August 2022). The similarity of homologs from various fungi was analyzed with the DNAMAN software package (version 5.2.2, Lynnon Biosoft, San Ramon, CA, USA). A BLAST algorithm was used to search for orthologs of Sec22 in different fungi. The resulting sequences were downloaded from the GenBank database for phylogenetic analysis with MEGA 7.0 software [40].

2.3. Targeted Gene Deletion of Aosec22 and Southern Blot Analysis

Aosec22 was disrupted by homologous recombination. Briefly, the upstream and downstream fragments of the *Aosec22* gene were amplified from *A. oligospora* DNA with paired primers (Table S1). The hygromycin-resistant gene *hph* amplified from the pCSN44 plasmid was used as a selection marker. The pRS426 plasmid was digested with *Eco*RI and *Xho*I, followed by co-transformation of the linearized plasmid and the amplified fragments into *S. cerevisiae* (FY834) by means of electroporation. The recombinant plasmid pRS426-AoSec22-hph was then isolated from the yeast plasmids. The target fragment gene for *Aosec22* disruption was amplified from the recombinant plasmid pRS426-AoSec22-hph using primers AoSec22-5f/AoSec22-3r (Table S1) and was transformed into *A. oligospora* using the protoplast transformation method, as described previously [41,42]. Briefly, the fungus *A. oligospora* was incubated in 100 mL of TG broth on a rotary shaker (160 rpm) at 28 °C for 36 h, then the mycelium was suspended in 10 mL MN solution (0.3 mol/L MgSO₄, 0.3 mol/L NaCl) containing 10 mg/mL of snailase (Solarbio, China) and cellulase (Solarbio, China) for 3–5 h in a shaking water bath (100 rpm) at 28 °C. The protoplasts were resuspended in 100 µL of MTC buffer (10 mM Tris-HCl, pH 7.5, 10 mM CaCl₂, 1 M MgSO₄). For transformation, circa 10⁷ protoplasts in 100 µL MTC were mixed with 10 µg of the *Aosec22* replacement fragment and incubated on ice for 40 min. 1 mL of PTC (10 mM Tris-HCl, pH 7.5, 10 mM CaCl₂, 20% w/v PEG 4000) were added and mixed gently. After incubation at room temperature for 1 h, 200–300 µL of the protoplast mixture was added to 5 mL of PDAS medium (PDA supplemented with 10 g/L molasses and 0.4 M saccharose) and poured into Petri dishes. The putative transformants were selected on PDAS medium containing 200 µg/mL of hygromycin B (Amresco, Solon, OH, USA) [43] and further verified by PCR and Southern blotting, as described previously [41].

2.4. Analysis of Vegetative Growth and Conidiation

The WT and mutant strains were incubated for 5-day radial growth on PDA, TYGA, and TG agar plates at 28 °C [41]. The spore yield of each strain was measured from the 15-day-old cultures grown on corn meal yeast extract (CMY) medium, as previously described [44,45]. Freshly harvested conidia and hyphae of WT and mutant strains were stained with 20 µg/mL of cell wall-specific calcofluor white (CFW, Sigma-Aldrich, St. Louis, MO, USA) or nucleus-specific 4',6-diamidino-2-phenylindole (DAPI, Sigma-Aldrich, USA), and visualized for hyphal morphology under an inverted fluorescence microscope [46,47].

2.5. Trap Induction and Bioassay

To induce trap formation, 50 µL suspensions (400 spores per µL) of the conidia collected from 15-day-old cultures were incubated on water agar plates at 28 °C for 3 days. Then, 400 nematodes were introduced to each plate for the induction of trap formation,

followed by microscopic observation of trap formation and nematode predation at a 12 h interval [45]. The traps were stained with 20 µg/mL CFW and visualized as aforementioned [47].

2.6. Microscopy Image Processing

For the staining of vacuole, the 3- to 5-day-old PDA cultures incubated at 28 °C were stained with 5 µM of 7-amino-4-chloromethylcoumarin (CMAC) (Thermo Fisher, Waltham, MA, USA) for 60 min on ice. After three washes with phosphate buffered saline, the stained hyphae were observed under a fluorescence microscopy [48]. For the staining of lipid droplets (LDs) and autophagosomes, hyphal samples were stained with 10 µg/mL of boron dipyrromethene (BODIPY) dye (Sigma-Aldrich, USA) and 10 µg/mL of monodansylcadaverine (MDC, Sigma-Aldrich, USA), respectively, for 30 min in the dark, followed by microscopic observation of the LDs and autophagosomes [37]. In addition, the ultrastructure of mycelial cells was revealed by transmission electron microscopy (TEM).

2.7. Analysis of Fungal Responses to Chemical Stressors

To determine the levels of stress resistance, the fungal strains were incubated on TG plates supplemented with or without (control) different concentrations of chemical stressors, including oxidative agents (H₂O₂ and menadione), osmotic agents (NaCl and sorbitol), and cell wall-perturbing agents (SDS and Congo red) at 28 °C for 5 days. Relative growth inhibition (RGI) values of the fungal strains were calculated as previously described [31,39]. Three replicates were analyzed for each treatment and control (TG medium alone).

2.8. Reverse Transcription Quantitative PCR (RT-qPCR) Analysis

The WT and mutants were inoculated on PDA plates at 28 °C and mycelia were collected on days 3, 5, and 7. Total RNA was isolated from each of the samples using an RNA extraction kit (Axygen, Jiangsu, China) and reversely transcribed into cDNA with a PrimeScript RT reagent kit (with genomic DNA; TaKaRa, Kusatsu, Japan). Primer pairs for the putative genes related to conidiation and lipid acid metabolism were designed (Table S2) and their transcript levels were assessed in the LightCycler 480 SYBR green I master mix (Applied Biosystems, Darmstadt, Germany). The β-tubulin gene was used as an internal standard. The relative transcript level of each gene was calculated using the threshold cycle ($2^{-\Delta\Delta CT}$) method [41].

2.9. Metabolomics Analysis

Three hyphal mass discs (7 mm) of each strain were incubated in PD broth for 7 days at 28 °C and 180 rpm, followed by mass collection through vacuum filtration [44]. The biomass was dried, weighed (WT, 3.14 g; Δ*Aosec22*, 2.89 g), and used to prepare extracts of the same concentration. Ethyl acetate (250 mL) was added to extract the fermentation broth and ultrasonic extraction was performed for 40 min. The fermentation broth was allowed to stand for 12 h and the crude extract was concentrated in ethyl acetate under vacuum [44]. The crude extract was dissolved in 500 µL of analytic-grade methanol and the solution was filtered through a 0.22 µm membrane filter for liquid chromatography–mass spectrometry (LC–MS) analysis. The metabolic profiles of the WT and mutant strains were compared using the Thermo Xcalibur software (Thermo Fisher Scientific). Untargeted metabolomics was performed using Compounds Discoverer 3.0 software (Thermo Fisher Scientific) [49].

2.10. Statistical Analysis

All experimental data were presented as the mean ± standard deviation (SD) of at least three replicated measurements. The differences between treatments were statistically evaluated by one-way analysis of variance using Prism 9.0 (GraphPad, San Diego, CA, USA). Differences were considered statistically significant if *p* value < 0.05.

3. Results

3.1. Sequence and Phylogenetic Analyses of AoSec22

Aosec22 encodes a protein of 215 amino acid residues with a theoretical MW of 23.5 kDa and a pI of 8.34. AoSec22 contains a conserved VARP interface domain and an R_SNARE_SEC22 domain shared by the SNC1 superfamily (Figure S1A). Meanwhile, AoSec22 shares higher sequence similarities with the orthologs of three other NT fungi (89.77–96.74%). In contrast, it shares moderate similarity (60.19–68.37%) with orthologs from other filamentous fungi, such as *Aspergillus fumigatus* and *F. graminearum*, and it also shares moderate similarity (51.87%) with *S. cerevisiae*. Moreover, a phylogenetic tree of orthologous Sec22 proteins from diverse fungi was constructed (Figure S1B) and the orthologous Sec22 proteins from NT fungi were divided into a branch.

3.2. Role of AoSec22 in Mycelial Growth and Nuclear Development

The gene *Aosec22* was disrupted using homologous recombination (Figure S2A,B) and the transformants were verified by PCR and Southern blot procedures (Figure S2C,D); five positive transformants were obtained and three mutants ($\Delta Aosec22-6$, $\Delta Aosec22-12$, and $\Delta Aosec22-20$) were randomly selected for this study. In assays for 5-day radial growth on PDA, TYGA, and TG plates at 28 °C. The growth of the $\Delta Aosec22$ mutants were remarkably slower than the WT strain (Figure 1A,B). Compared to the WT strain, the $\Delta Aosec22$ mutants showed not only more septa in hyphae and shorter length in hyphal cells (Figure 1C,D), but also fewer nuclei in hyphal cells of the mutants (3–8 nuclei per cell) versus the WT strain (9–13 nuclei per cell) (Figure 1C,E).

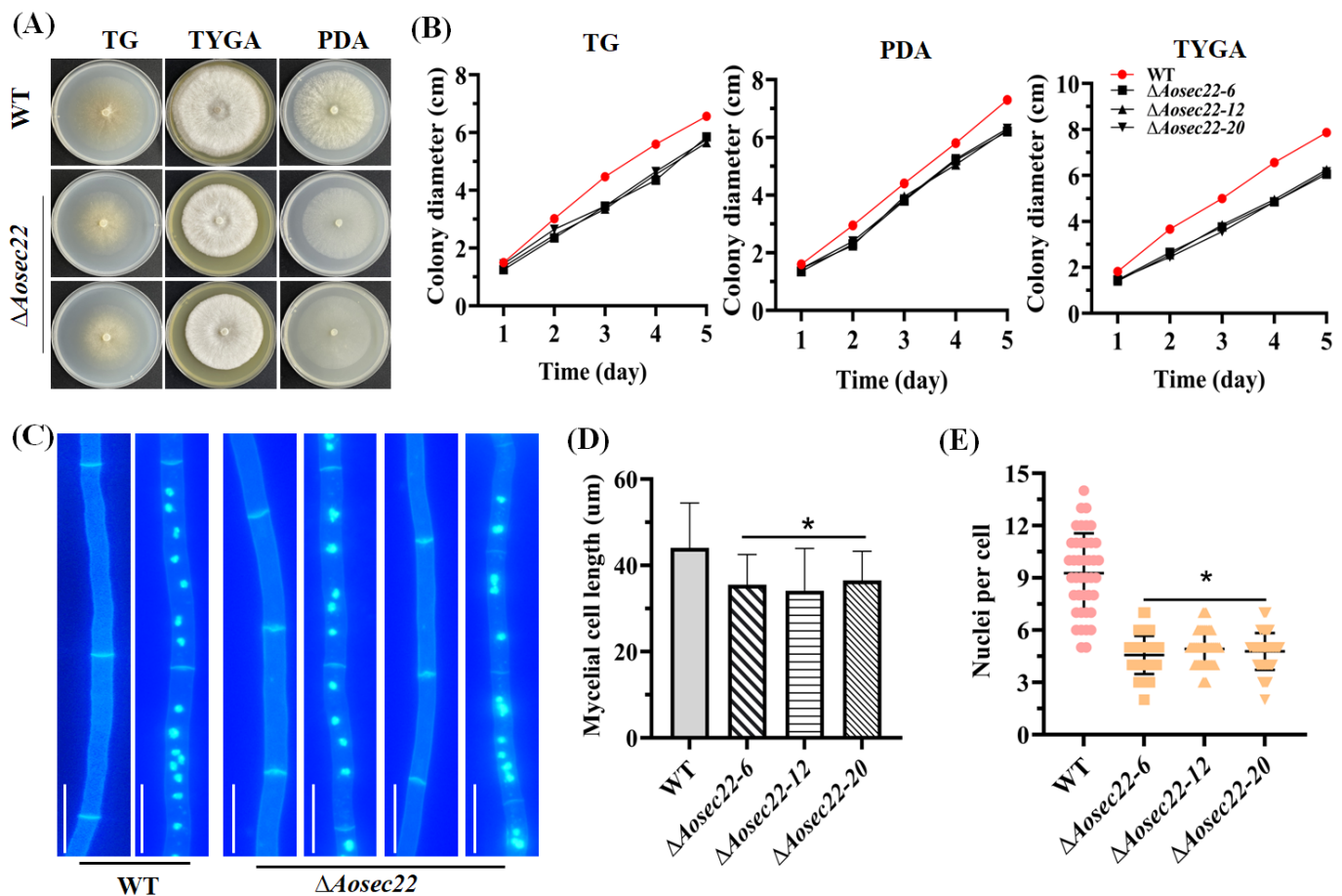


Figure 1. Comparison of mycelial growth of wild-type (WT) and mutant strains in *A. oligospora*. (A) Colony morphology of fungal strains incubated for 5 days on PDA, TG, and TYGA plates at 28 °C.

(B) Diameters of fungal colonies in (A). (C) Hyphae of the WT and mutant strains stained with calcofluor white (CFW) and 4',6-diamidino-2-phenylindole (DAPI) after 7-day incubation on CMY. One hundred hyphal cells were randomly selected for the counts of nuclei. Bar: 10 μ m. (D,E) Length of hyphal cells and count of nuclei in (C). Measurements represent the average of three independent experiments. The asterisk indicates a significant difference between the mutant and WT strains ($p < 0.05$).

3.3. Essentiality of AoSec22 for Conidiation

The disruption of *AoSec22* resulted in reduced conidial production (Figure 2A). The spore yields of the WT and the Δ *AoSec22* mutant strains were estimated to be 4.5×10^5 and 1.5×10^5 spores/mL, respectively (Figure 2B). Moreover, spore germination was slowed down in the Δ *AoSec22* mutants versus the WT strain during normal incubation (Figure 2C). Among six sporulation-related genes analyzed during vegetative growth and sporulation, four (*fluG*, *velB*, *brlA*, and *abaA*) were remarkably downregulated ($p < 0.05$) on day 3 (vegetative growth), especially *brlA*, which was significantly downregulated on days 3, 5, and 7. On the 5th day, four genes (*velB*, *brlA*, *wetA*, and *abaA*) were significantly downregulated, whereas *fluG* and *flbC* did not show a significant difference on the 5th day (Figure 2D). Additionally, four genes (*flbC*, *velB*, *brlA*, and *wetA*) were downregulated on day 7. The WT strain produced an obovoid spore, with one septum formed near the base of the spore; in contrast, 61% of the conidia of the Δ *AoSec22* mutant were morphologically abnormal; these spores lost their septa and became smaller compared with those of the WT strain (Figure 2E).

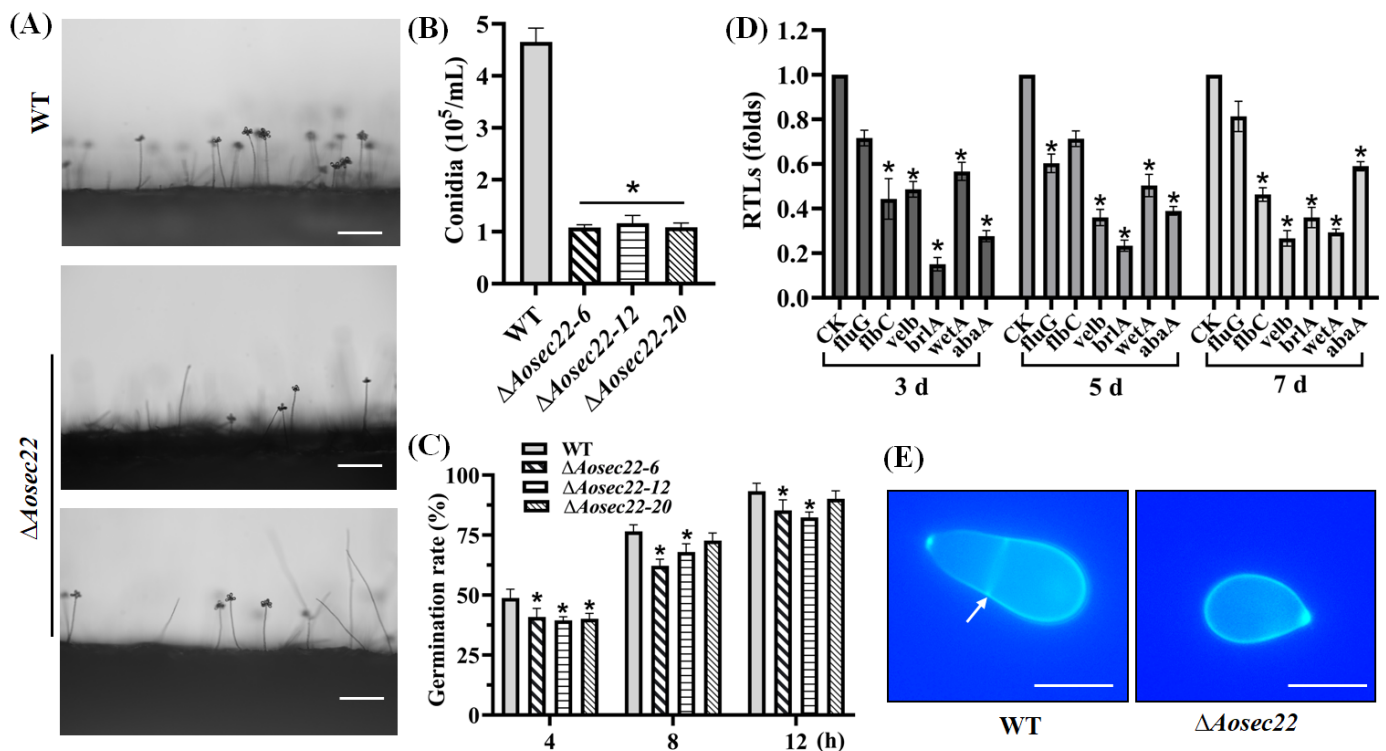


Figure 2. Role of *AoSec22* in conidiation and conidial morphology. (A) Microscopic images (scale: 50 μ m) for conidiation of the WT and mutant strains on PDA. (B) Spore yields assessed from 15-days-old cultures. (C) Spore germination rate during normal incubation. (D) Relative transcription levels (RTLs) of sporulation-related genes in the WT and mutant strains. An asterisk (B–D) indicates a significant difference between the mutant and WT strains ($p < 0.05$). CK was used as the standard (RTL = 1) for statistical analysis of the RTL of each gene under a given condition. (E) Microscopic images (scale: 10 μ m) of conidia stained with calcofluor white (CFW). The white arrow indicates the septum.

3.4. *AoSec22* Is Required for Trap Morphogenesis

To examine if *AoSec22* is involved in *A. oligospora* trap morphogenesis, we compared phenotypic differences between the WT and the mutants upon exposure to *C. elegans* at different time points. The $\Delta Aosec22$ mutant formed far fewer traps severely compromised in the development of three-dimensional structures than the WT strain (Figure 3A–C); the traps of the WT strain consisted of 5–8 mycelial loops, contrasting with only 2–3 loops in the mutants' traps at 48 h post-induction (hpi). Consequently, the number of traps in the $\Delta Aosec22$ mutant decreased to 35–50% of those in WT (Figure 3C). At 12 and 24 hpi, the $\Delta Aosec22$ mutant was less capable of capturing nematodes than WT, but its capability was largely restored at 36 and 48 hpi (Figure 3D).

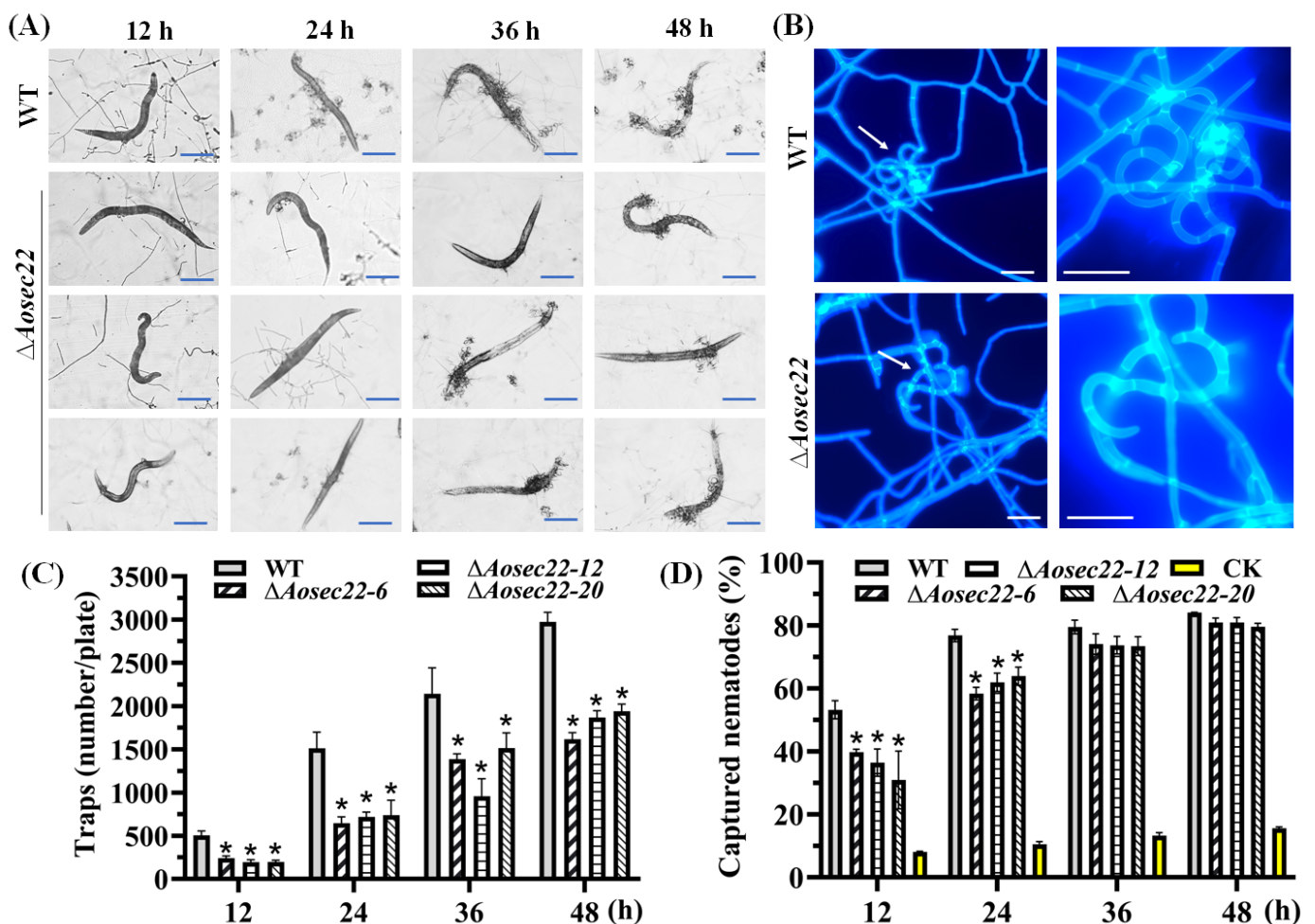


Figure 3. Role of *AoSec22* in trap formation, nematocidal activity, and trap morphology. (A,B) Microscopic images for trap formation and nematode predation at different time points and enlarged traps at 48 h. White arrows: traps. Bar: 100 μ m in (A) and 10 μ m in (B). (C) Counts of traps produced by WT and $\Delta Aosec22$ mutant strains at 12, 24, 36, and 48 h. (D) Percentages of nematodes captured by WT and $\Delta Aosec22$ mutant strains at 12, 24, 36, and 48 h. An asterisk (C,D) indicates a significant difference between the $\Delta Aosec22$ mutant and the WT strain (Tukey's HSD, $p < 0.05$).

3.5. *AoSec22* Plays an Important Role in Fatty Acid Utilization

Revealed by hyphal staining and imaging, the mutants' LDs were enlarged remarkably compared with the WT counterparts (Figure 4A). In addition, large LDs were also present in the $\Delta Aosec22$ mutants' TEM images (Figure 4B). To reveal the effect of *AoSec22* on fatty acid utilization, seven genes involved in fatty acid oxidation were analyzed, including the coding genes of 3-ketoacyl-CoA ketothiolase (*AOL_s00210g122*), 3-hydroxybutyryl-

CoA dehydrogenase (AOL_s00110g113), acyl-CoA dehydrogenase (AOL_s00079g276), 3-oxoacyl- [acyl-carrier protein] reductase (AOL_s00004g288), phosphatidylinositol transporter (AOL_s00081g51), peroxisomal multi-functional beta-oxidation protein (AOL_s00054g29), and peroxisomal ABC transporter (AOL_s00004g606). As a result, only one gene (AOL_s00054g29) was upregulated in the mutant on day 3, while three and six genes were downregulated in the $\Delta Aosec22$ mutant on days 5 and 7, respectively (Figure 4C).

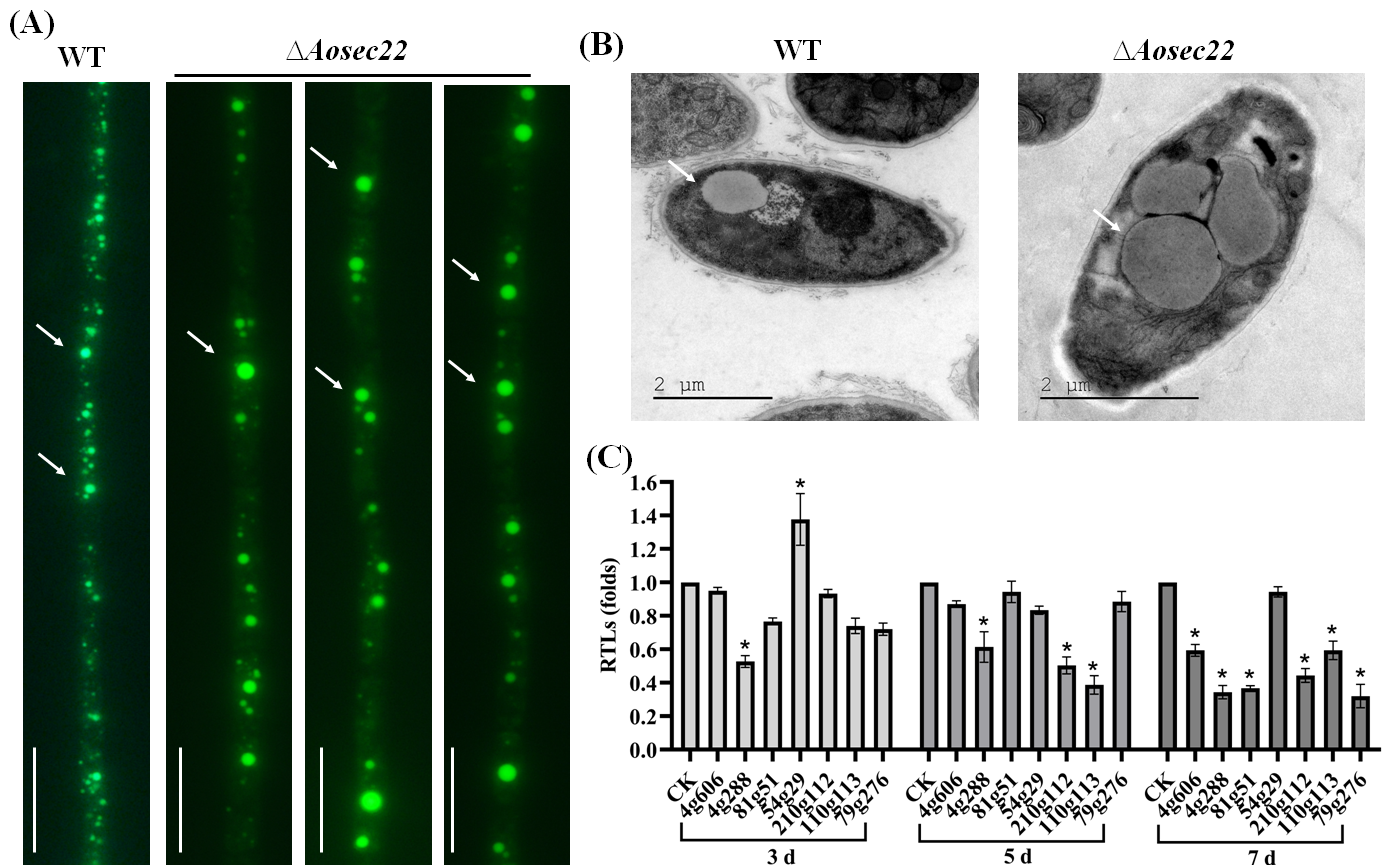


Figure 4. Impact of *Aosec22* disruption on morphology of lipid droplets (LDs) and transcription of genes involved in fatty acid oxidation. (A,B) Microscopic (scale: 10 μ m) and SEM images of LDs in hyphal cells. LDs in (A) were stained with 10 μ g/mL BODIPY dye. Arrows: LDs. Bar: 10 μ m. (C) Relative transcript levels (RTLs) of genes related to fatty acid oxidation between $\Delta Aosec22$ mutant and WT strains on days 3, 5, and 7. CK (standardized to 1) was used as a standard. An asterisk indicates a significant difference between $\Delta Aosec22$ mutant and WT strains (Tukey's HSD, $p < 0.05$).

3.6. *AoSec22* Regulates Autophagy and Vacuole Assembly

Stained with MDC, autophagosomes were clearly observed in the hyphae of the WT and the $\Delta Aosec22$ mutant. The WT mycelia contained many autophagosomes distributed in a punctate pattern, whereas far fewer autophagosomes appeared in the hyphal cells of the $\Delta Aosec22$ mutant and distributed in a dispersed pattern (Figure 5A). To reveal the effect of *AoSec22* on vacuole assembly, we stained the WT and mutant hyphae with CMAC, a fluorescent dye specific to vacuoles [48]. The vacuoles of $\Delta Aosec22$ were small and fragmented, whereas the vacuoles of the WT were regular and large (Figure 5B). TEM images also demonstrated more vacuoles in the hyphal cells of $\Delta Aosec22$ than of WT (Figure 5C).

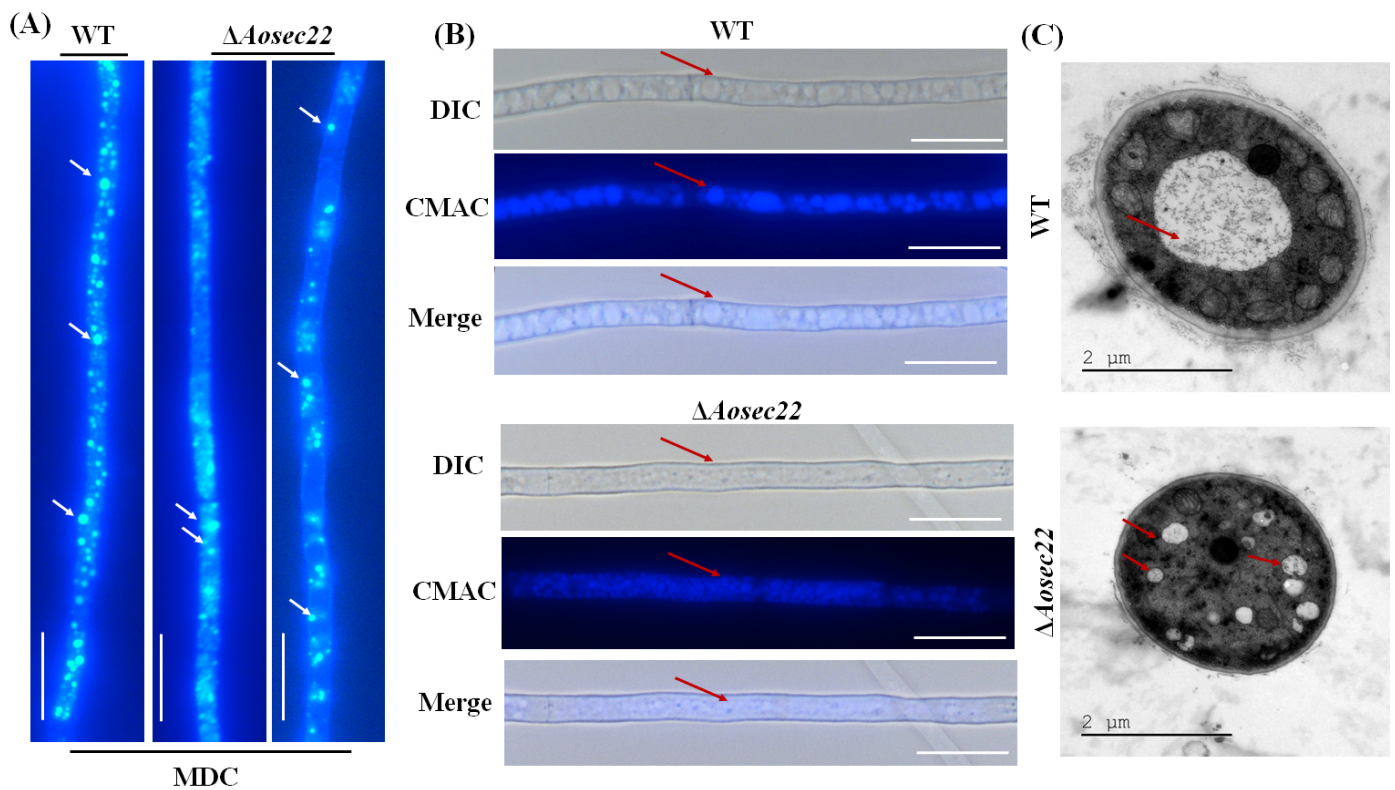


Figure 5. Impact of *Aosec22* disruption on autophagy and vacuolar assembly. (A) Microscopic images (scale: 10 μm) of autophagosomes (arrowed) in hyphal cells stained with MDC. (B) Microscopic images (scale: 10 μm) of vacuoles in hyphal cells stained with CMAC. (C) TEM images of vacuoles in ultrathin sections of hyphal cells. Red arrows: vacuole.

3.7. Role of *AoSec22* in Stress Response

In stress assays, the mycelial growth of the $\Delta Aosec22$ mutant was suppressed in the presence of cell wall-perturbing agents (Congo red and SDS), and its RGI values were significantly increased ($p < 0.05$) by Congo red (0.05–0.1 mg/mL) and SDS (0.1–0.3%) (Figure 5A,B). Meanwhile, the $\Delta Aosec22$ mutant also showed increased sensitivity to 0.2 and 0.3 M NaCl and 0.75 M sorbitol (Figure 6A,B). However, H_2O_2 and menadione had no influence on the mycelial growth of $\Delta Aosec22$ mutant, except under 0.75 mM menadione, when the RGI was increased significantly (Figure S3).

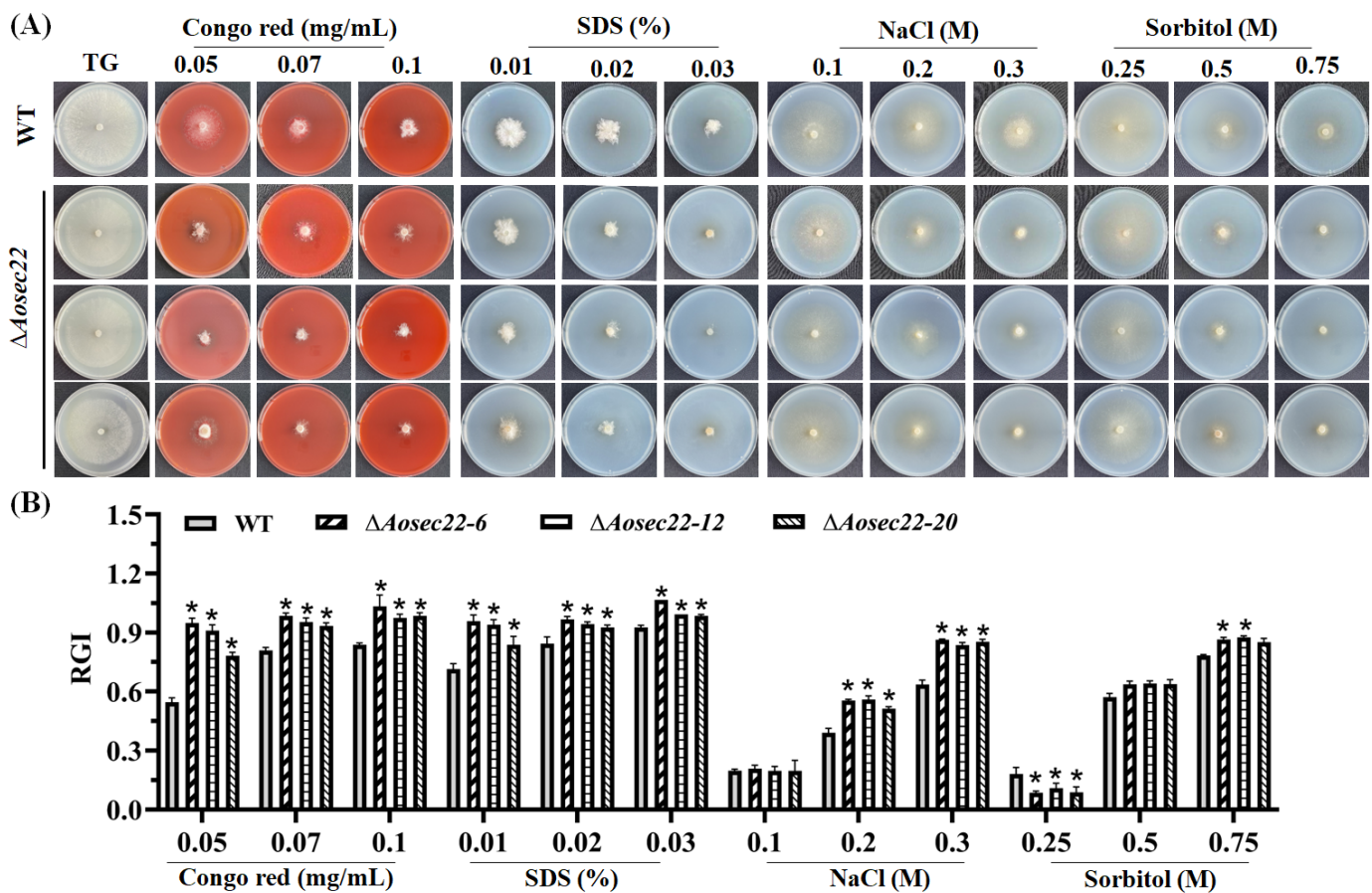


Figure 6. Comparison of stress responses between WT and $\Delta Aosec22$ strains. (A) Colonial morphology of fungal strains under osmotic and cell wall-perturbing stress. (B) Relative growth inhibition (RGI) of fungal colonies after 6-day incubation at 28 °C on TG plates supplemented with indicated concentrations of Congo red, SDS, NaCl, and sorbitol. An asterisk indicates a significant difference between $\Delta Aosec22$ mutant and the WT strain (Tukey's HSD, $p < 0.05$).

3.8. *AoSec22* Is Involved in the Regulation of Secondary Metabolism

The mycelia of the $\Delta Aosec22$ mutant turned red after 10-day incubation on PDA (Figure S4A). In addition, LC-MS analysis revealed the difference in the mass and number of compounds in the extracts of the WT and mutant cultures. The WT and mutant strains' chromatographic spectra differed in the peak areas of several compounds (Figure 7A). A cluster heatmap showed that the metabolic profiles of the $\Delta Aosec22$ mutant were different from those of the WT, and more metabolic pathways were upregulated in the $\Delta Aosec22$ mutant (Figure 7B). A volcano plot analysis showed that 1230 compounds were downregulated and 4717 compounds were upregulated in the $\Delta Aosec22$ mutant compared to the WT strain (Figure 7C). The differential metabolic pathways mainly focused on the metabolic pathways, the biosynthesis of secondary metabolites, the degradation of aromatic compounds, steroid hormone biosynthesis, and microbial metabolism in diverse environments (Figure 7D). Moreover, arthrobotrisins, specific metabolites produced by *A. oligospora* and other NT fungi, were detected in the WT and mutant strains (diagnostic fragments of ions at 139, 393, and 429 m/z under negative ion conditions) [50,51], and their peak areas were remarkably increased in the mutants (Figures S4B,C).

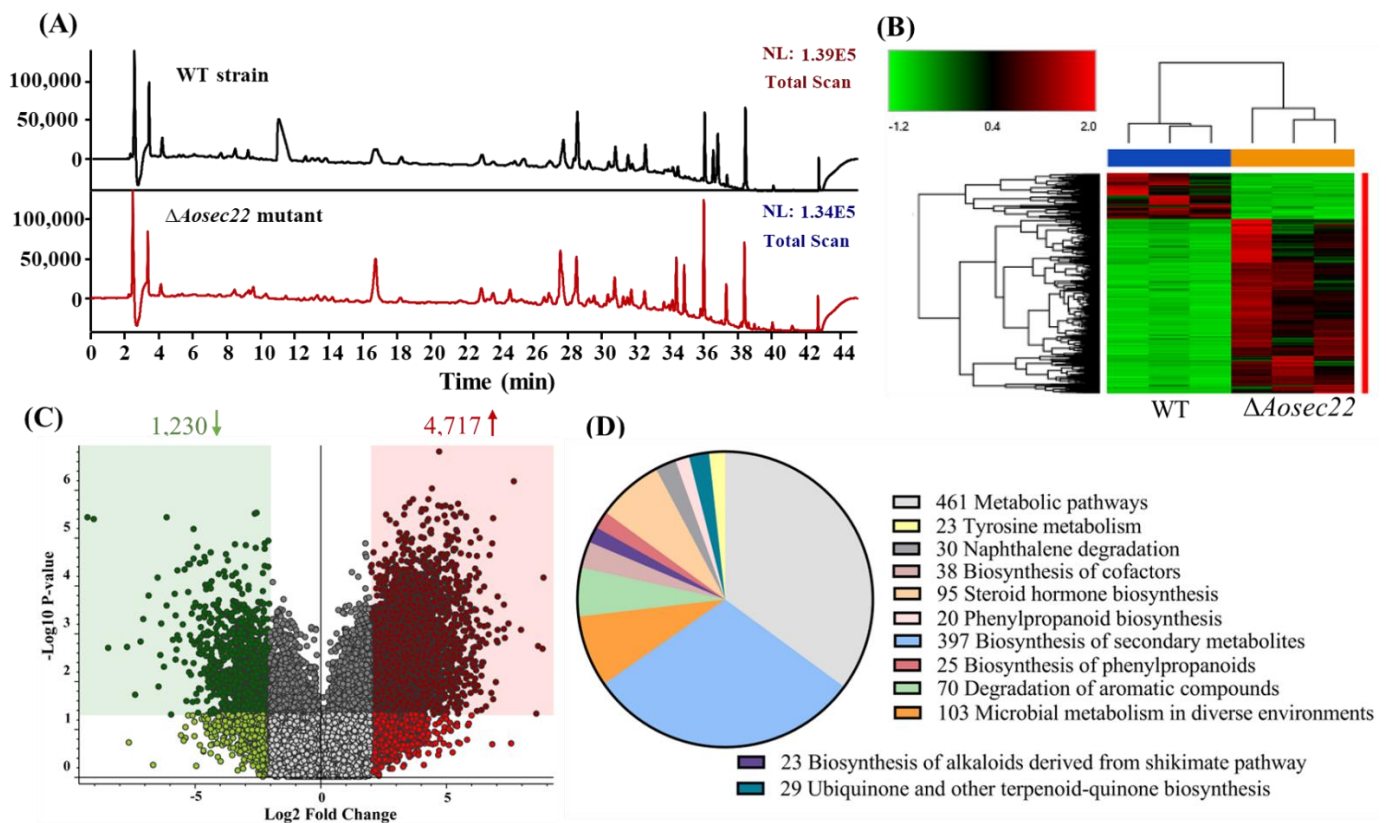


Figure 7. Comparison of metabolic profiling between WT and $\Delta Aosec22$ mutant strains. (A) Comparison of high-performance liquid chromatography profiles of the WT and $\Delta Aosec22$ mutant strains. (B) Heatmap for upregulated and downregulated metabolic pathways between $\Delta Aosec22$ mutant and WT strains determined via KEGG enrichment. (C) Volcano plot of differential metabolites between $\Delta Aosec22$ mutant and WT strains. (D) The number of downregulated and upregulated KEGG pathways in $\Delta Aosec22$ mutant.

4. Discussion

Sec22 is a member of the SNARE family of proteins, and its homologs play a major role in vesicle trafficking and membrane fusion, which are essential processes for normal cellular functions and homeostasis, and have diverse biological roles in different organisms [10,19]. As presented above, AoSec22 has pleiotropic roles in the lifecycle of *A. oligospora*. Its role in vegetative growth, sporulation, stress response, trap formation, lipid metabolism, vacuole assembly, and secondary metabolism is discussed below.

The deletion of *Aosec22* exerted a profound effect on fungal growth and morphology. Aerial mycelia became thinner and sparser, accompanied by increased septa, reduced cell length, and fewer nuclei in each hyphal cell. The $\Delta Aosec22$ mutant's conidiation capacity was lowered and its spore morphology was abnormal. Our observations were consistent with previous observations in *M. oryzae* [23] and *F. graminearum* [24]. In *F. graminearum*, FgSec22 was reported to be indispensable for normal conidiation and conidial morphology [24]. In the present study, the reduced conidiation level correlated with transcriptional repression of several asexual development-required genes, particularly *brlA*, *abaA*, and *wetA*, crucial for the conidiation of *Beauveria bassiana*, *Monascus ruber*, and other fungi [52–54]. In *B. bassiana*, loss-of-function mutations of *wetA* have compromised conidiation capacity by 98% [55]. Moreover, BrlA and AbaA are highly conserved activators of asexual development in filamentous fungi [56,57]. BrlA and AbaA are indispensable for aerial conidiation in *Metarhizium robertii* as well as in *B. bassiana* [52,54]. These results indicate that Sec22 plays a conserved role in sustaining mycelial radial growth, aerial

hyphal development, and conidiation in filamentous fungi, and is also crucial for the development of the hyphal septation and nuclear division in *A. oligospora*.

Previous studies have shown that SNAREs are essential for pathogenicity in several plant pathogenic fungi, such as *M. oryzae* [23], *F. graminearum* [24,25], *V. dahliae* [26], and *Colletotrichum fructicola* [58]. In *F. graminearum*, the deletion of *Fgsec22* resulted in reduced pathogenicity [24]. Similarly, *CfVam7* is also required for appressorium formation and homotypic vacuole fusion, which are vital for host infection of *C. fructicola* [58]. In the other NT fungus *D. dactyloides*, deletion of *Ddvam7* significantly impaired trap formation and markedly decreased nematode-trapping ability [38]. In our study, the $\Delta Aosec22$ mutant was capable of forming traps in the presence *C. elegans*, suffered a decrease in the number of formed traps, and hence displayed a defect in developing proper three-dimensional structures. Therefore, the traps formed by the $\Delta Aosec22$ mutant had fewer loops, implicating an impaired capability of capturing nematodes. These present and previous studies indicate SNAREs are required not only for the pathogenicity of phytopathogenic fungi but also for the development of traps in *D. dactyloides* and *A. oligospora*.

Aside from the growth and trap defects under normal culture conditions, the $\Delta Aosec22$ mutant was hypersensitive to cell wall-perturbing and osmotic stresses. Previously, the $\Delta Mosec22$ mutant showed increased sensitivity to cell wall stressors and H_2O_2 [38]. The $\Delta Movam7$ mutant exhibited weakened cell wall and membrane, which were coupled with an abnormal distribution of chitins [59]. *Sec22* is involved in the regulation of chitin synthesis in *S. cerevisiae* [60]. Chitin is one of the most important carbohydrates in the fungal cell wall, which maintains structural integrity [61,62]. In *F. graminearum*, the $\Delta Fgvam7$ mutant was insensitive to some salt and osmotic agents, but hypersensitive to other osmotic and cell wall stressors; moreover, the $\Delta Fgsec22$ mutant showed increased sensitivity to cell wall stressors [24,63]. These findings indicate that SNAREs, such as *Sec22* orthologs, are functional in fungal stress responses, especially in cell wall-perturbing and osmotic stresses of *A. oligospora*.

SNAREs regulate autophagosome formation and are involved in exocytosis in yeast; the endosomal *Tlg2*, *Sec22*, and *Ykt6* interact with the *Sso1*-*Sec9* complex required for normal *Atg9* trafficking [64,65]. *Sec22* is not directly involved in exocytosis, as it participates in autophagosome–vacuole fusion and the regulation of the tubular network formation of *Atg9* [65,66]. In this study, both autophagosomes and LDs were remarkably reduced in the hyphal cells of the $\Delta Aosec22$ mutant, accompanied by enlarged LDs. The altered LDs correlated with transcriptional repression of several genes involved in fatty acid oxidation, such as 3-ketoacyl-CoA ketothiolase (AOL_s00210g122), 3-hydroxybutyryl-CoA dehydrogenase (AOL_s00110g113), and acyl-CoA dehydrogenase (AOL_s00079g276). In contrast, the transcript of AOL_s00054g29 was upregulated on the third day, whereas its expression showed no obvious change in the $\Delta Aosec22$ mutant compared to the WT on the fifth and seventh days. Previously, knockout mutations of SNAREs obliterated tubular network formation and resulted in small *Atg9*-containing vesicles to stop homotypic fusion events [64,67]. Fungal vacuoles are dynamic, as they undergo a continuous balance of fission and fusion to allow changes in shape, size, and number, and are vital for fungal morphogenesis [68,69]. In this study, the absence of *Aosec22* resulted in a defect in vacuole assembly, since the vacuoles became small and fragmented. Similarly, *MoVam7* and *MoSec22* are involved in maintaining the shapes of vacuoles in *M. oryzae* [23,59]. The $\Delta Movam7$ mutant displayed more smaller vacuoles, as seen in the $\Delta vam7$ mutant of *S. cerevisiae* [59,70]. In the $\Delta Ddvam7$ mutant, smaller vacuoles were present in the hyphae and uninflated ring cells, making it unable to form large vacuoles in the inflated ring cells [38]. Vacuoles are crucial for nutrient transport in fungi and abnormal vacuoles may interfere with the formation of traps [38]. The mechanisms underlying the formation of large vacuoles and the molecules directly involved remain to be further explored. These findings reveal that *Sec22* is required for vacuole assembly and is also crucial for LD utilization and autophagosome formation in *A. oligospora*.

SNAREs are also involved in secondary metabolism in filamentous fungi. In *F. graminearum*, DON production was significantly reduced (by 90%) in the $\Delta Fgsec22$ mutant strain [24]. In the present study, the loss of *Aosec22* caused the change of colony color and a significant increase in metabolites. KEGG analysis revealed that the differential compounds were enriched in metabolism and related processes, such as the biosynthesis of secondary metabolites and the degradation of aromatic compounds. Moreover, arthrotrisin is a type of polyketide synthase–terpenoid synthase hybrid metabolites produced by *A. oligospora* and other NT fungi, and are known to inhibit hyphal growth and trap formation [50,51,71,72]. In this study, the arthrotrisin content was evidently increased in the $\Delta Aosec22$ mutant, coinciding with its reduced growth and trap formation. Thus, *AoSec22* may play an important role in the mediation of secondary metabolism in *A. oligospora*.

5. Conclusions

Our results indicate that the SNARE protein *AoSec22* plays a vital role in mycelial growth, conidiation, stress response, trap formation, and secondary metabolism in *A. oligospora*. Moreover, *AoSec22* participates in the regulation of vacuole assembly and LD morphology. These findings expand the knowledge on the biological functions of the SNARE proteins in NT fungi and provides a basis for future studies on molecular mechanisms underlying vacuole assembly and trap development.

Supplementary Materials: The following supporting information can be downloaded at: <https://www.mdpi.com/article/10.3390/jof9010075/s1>. Figure S1: Multiple sequence alignment and phylogenetic analysis of WT and $\Delta Aosec22$ mutant strains; Figure S2: Knockout and verification of the genes *Aosec22* in *A. oligospora*; Figure S3: Comparison of oxidative stress responses between WT and $\Delta Aosec22$ mutant strains; Figure S4: Comparison of the color of colony and the content of arthrotrisin; Table S1: List of primers for gene disruption used in this study; Table S2: Paired primers for RT-qPCR analysis of genes associated with phenotypes such as conidiation and fatty acid oxidation in *A. oligospora*.

Author Contributions: J.Y. conceived and designed the study. Y.Z. and D.Z. performed the experiments. N.B., Q.L. and N.Z. analyzed the data. Y.Z. and J.Y. contributed to manuscript preparation and revision. All authors have read and agreed to the published version of the manuscript.

Funding: Funding for this study was provided by the National Natural Science Foundation of China (no. 31960556) and the Applied Basic Research Foundation of Yunnan Province (no. 202001BB050004).

Institutional Review Board Statement: Not applicable.

Informed Consent Statement: Not applicable.

Data Availability Statement: Not applicable.

Acknowledgments: We are grateful to Microbial Library of the Germplasm Bank of Wild Species from Southwest China for preserving and providing experimental strains, and Guo Ying-qi and Wu Xingcai (Kunming Institute of Zoology, Chinese Academy of Sciences) for their help with taking and analyzing TEM images. We are grateful to Mingguang Feng (Zhejiang University, China) for his valuable comments and critical discussions.

Conflicts of Interest: We declare that we have no conflict of interests.

References

1. Palade, G. Intracellular aspects of the process of protein secretion. *Science* **1975**, *189*, 867. [[CrossRef](#)] [[PubMed](#)]
2. Friedman, J.R.; Voeltz, G.K. The ER in 3D: A multifunctional dynamic membrane network. *Trends Cell Biol.* **2011**, *21*, 709–717. [[CrossRef](#)] [[PubMed](#)]
3. Chino, H.; Mizushima, N. ER-phagy: Quality control and turnover of endoplasmic reticulum. *Trends Cell Biol.* **2020**, *30*, 384–398. [[CrossRef](#)] [[PubMed](#)]
4. Schwarz, D.S.; Blower, M.D. The endoplasmic reticulum: Structure, function and response to cellular signaling. *Cell. Mol. Life Sci.* **2016**, *73*, 79–94. [[CrossRef](#)] [[PubMed](#)]

5. Lamb, C.A.; Yoshimori, T.; Tooze, S.A. The autophagosome: Origins unknown, biogenesis complex. *Nat. Rev. Mol. Cell Biol.* **2013**, *14*, 759–774. [[CrossRef](#)]
6. Witkos, T.M.; Lowe, M. Recognition and tethering of transport vesicles at the Golgi apparatus. *Curr. Opin. Cell Biol.* **2017**, *47*, 16–23. [[CrossRef](#)]
7. Bonifacino, J.S.; Glick, B.S. The mechanisms of vesicle budding and fusion. *Cell* **2004**, *116*, 153–166. [[CrossRef](#)]
8. Jahn, R.; Scheller, R.H. SNAREs—engines for membrane fusion. *Nat. Rev. Mol. Cell Biol.* **2006**, *7*, 631–643. [[CrossRef](#)]
9. Han, J.; Pluhackova, K.; Böckmann, R.A. The multifaceted role of SNARE proteins in membrane fusion. *Front. Physiol.* **2017**, *8*, 5.
10. Zhao, Y.; Holmgren, B.T.; Hinas, A. The conserved SNARE SEC-22 localizes to late endosomes and negatively regulates RNA interference in *Caenorhabditis elegans*. *RNA* **2017**, *23*, 297–307.
11. Südhof, T.C.; Rothman, J.E. Membrane fusion: Grappling with SNARE and SM proteins. *Science* **2009**, *323*, 474–477. [[CrossRef](#)]
12. Bao, J.; Huang, M.; Petranovic, D.; Nielsen, J. Balanced trafficking between the ER and the Golgi apparatus increases protein secretion in yeast. *AMB Express* **2018**, *8*, 37. [[CrossRef](#)]
13. Adnan, M.; Fang, W.; Sun, P.; Zheng, Y.; Abubakar, Y.S.; Zhang, J.; Lou, Y.; Zheng, W.; Lu, G.D. R-SNARE FgSec22 is essential for growth, pathogenicity and DON production of *Fusarium graminearum*. *Curr. Genet.* **2020**, *66*, 421–435. [[CrossRef](#)]
14. Fasshauer, D.; Sutton, R.B.; Brunger, A.T.; Jahn, R. Conserved structural features of the synaptic fusion complex: SNARE proteins reclassified as Q- and R-SNAREs. *Proc. Natl. Acad. Sci. USA* **1998**, *95*, 15781–15786. [[CrossRef](#)]
15. Bas, L.; Papinski, D.; Licheva, M.; Torggler, R.; Rohringer, S.; Schuschnig, M.; Kraft, C. Reconstitution reveals Ykt6 as the autophagosomal SNARE in autophagosome-vacuole fusion. *J. Cell Biol.* **2018**, *217*, 3656–3669. [[CrossRef](#)]
16. Bruinsma, S.; James, D.J.; Serrano, M.Q.; Esquibel, J.; Woo, S.S.; Kielar-Grevstad, E.; Crummy, E.; Qurashi, R.; Kowalchyk, J.A.; Martin, T.F.J. Small molecules that inhibit the late stage of Munc13-4-dependent secretory granule exocytosis in mast cells. *J. Biol. Chem.* **2018**, *293*, 8217–8229. [[CrossRef](#)]
17. Li, X.; Wu, Y.; Shen, C.; Belenkaya, T.Y.; Ray, L.; Lin, X. Drosophila p24 and Sec22 regulate Wingless trafficking in the early secretory pathway. *Biochem. Biophys. Res. Commun.* **2015**, *463*, 483–489. [[CrossRef](#)]
18. Flanagan, J.J.; Mukherjee, I.; Barlowe, C. Examination of Sec22 homodimer formation and role in SNARE-dependent membrane fusion. *J. Biol. Chem.* **2015**, *290*, 10657–10666. [[CrossRef](#)]
19. Zhao, X.; Yang, H.; Liu, W.; Duan, X.; Shang, W.; Xia, D.; Tong, C. Sec22 regulates endoplasmic reticulum morphology but not autophagy and is required for eye development in *Drosophila*. *J. Biol. Chem.* **2015**, *290*, 7943–7951. [[CrossRef](#)]
20. Dräxl, S.; Müller, J.; Li, W.B.; Michalke, B.; Scherb, H.; Hense, B.A.; Tschiersch, J.; Kanter, U.; Schäffner, A.R. Caesium accumulation in yeast and plants is selectively repressed by loss of the SNARE Sec22p/SEC22. *Nat. Commun.* **2013**, *4*, 2092. [[CrossRef](#)]
21. El-Kasmi, F.; Pacher, T.; Strompen, G.; Stierhof, Y.D.; Müller, L.M.; Koncz, C.; Mayer, U.; Jürgens, G. Arabidopsis SNARE protein SEC22 is essential for gametophyte development and maintenance of Golgi-stack integrity. *Plant J.* **2011**, *66*, 268–279. [[CrossRef](#)] [[PubMed](#)]
22. Paek, I.; Orci, L.; Ravazzola, M.; Erdjument-Bromage, H.; Amherdt, M.; Tempst, P.; Söllner, T.H.; Rothman, J.E. ERS-24, a mammalian v-SNARE implicated in vesicle traffic between the ER and the Golgi. *J. Cell Biol.* **1997**, *137*, 1017–1028. [[CrossRef](#)] [[PubMed](#)]
23. Hay, J.C.; Chao, D.S.; Kuo, C.S.; Scheller, R.H. Protein interactions regulating vesicle transport between the endoplasmic reticulum and Golgi apparatus in mammalian cells. *Cell* **1997**, *89*, 149–158. [[CrossRef](#)] [[PubMed](#)]
24. Song, W.; Dou, X.; Qi, Z.; Wang, Q.; Zhang, X.; Zhang, H.; Guo, M.; Dong, S.; Zhang, Z.; Wang, P.; et al. R-SNARE homolog MoSec22 is required for conidiogenesis, cell wall integrity, and pathogenesis of *Magnaporthe oryzae*. *PLoS ONE* **2010**, *5*, e13193. [[CrossRef](#)] [[PubMed](#)]
25. Adnan, M.; Islam, W.; Noman, A.; Hussain, A.; Anwar, M.; Khan, M.U.; Akram, W.; Ashraf, M.F.; Raza, M.F. Q-SNARE protein FgSyn8 plays important role in growth, DON production and pathogenicity of *Fusarium graminearum*. *Microb. Pathog.* **2020**, *140*, 103948. [[CrossRef](#)]
26. Wang, J.; Tian, L.; Zhang, D.D.; Short, D.P.G.; Zhou, L.; Song, S.S.; Liu, Y.; Wang, D.; Kong, Z.Q.; Cui, W.Y.; et al. SNARE-encoding genes *VdSec22* and *VdSso1* mediate protein secretion required for full virulence in *Verticillium dahliae*. *Mol. Plant Microbe Interact.* **2018**, *31*, 651–664. [[CrossRef](#)]
27. Zhu, M.C.; Li, X.M.; Zhao, N.; Yang, L.; Zhang, K.Q.; Yang, J.K. Regulatory mechanism of trap formation in the nematode-trapping fungi. *J. Fungi* **2022**, *8*, 406. [[CrossRef](#)]
28. Jiang, X.; Xiang, M.; Liu, X. Nematode-trapping fungi. *Microbiol. Spectr.* **2017**, *5*, FUNK-0022-2016. [[CrossRef](#)]
29. Yang, J.; Wang, L.; Ji, X.; Feng, Y.; Li, X.; Zou, C.; Xu, J.; Ren, Y.; Mi, Q.; Wu, J.; et al. Genomic and proteomic analyses of the fungus *Arthrobotrys oligospora* provide insights into nematode-trap formation. *PLoS Pathog.* **2011**, *7*, e1002179. [[CrossRef](#)]
30. Nordbring-Hertz, B. Morphogenesis in the nematode-trapping fungus *Arthrobotrys oligospora* an extensive plasticity of infection structures. *Mycologist* **2004**, *18*, 125–133. [[CrossRef](#)]
31. Zhen, Z.; Xing, X.; Xie, M.; Yang, L.; Yang, X.; Zheng, Y.; Chen, Y.; Ma, N.; Li, Q.; Zhang, K.Q.; et al. MAP kinase Slt2 orthologs play similar roles in conidiation, trap formation, and pathogenicity in two nematode-trapping fungi. *Fungal Genet. Biol.* **2018**, *116*, 42–50. [[CrossRef](#)]
32. Yang, C.T.; Vidal-Diez de Ulzurrun, G.; Gonçalves, A.P.; Lin, H.C.; Chang, C.W.; Huang, T.Y.; Chen, S.A.; Lai, C.K.; Tsai, I.J.; Schroeder, F.C.; et al. Natural diversity in the predatory behavior facilitates the establishment of a robust model strain for nematode-trapping fungi. *Proc. Natl. Acad. Sci. USA* **2020**, *117*, 6762–6770. [[CrossRef](#)]

33. Bai, N.; Zhang, G.; Wang, W.; Feng, H.; Yang, X.; Zheng, Y.; Yang, L.; Xie, M.; Zhang, K.Q.; Yang, J. Ric8 acts as a regulator of G-protein signalling required for nematode-trapping lifecycle of *Arthrobotrys oligospora*. *Environ. Microbiol.* **2022**, *24*, 1714–1730. [[CrossRef](#)]
34. Ma, N.; Zhao, Y.; Wang, Y.; Yang, L.; Li, D.; Yang, J.; Jiang, K.; Zhang, K.Q.; Yang, J. Functional analysis of seven regulators of G protein signaling (RGSs) in the nematode-trapping fungus *Arthrobotrys oligospora*. *Virulence* **2021**, *12*, 1825–1840. [[CrossRef](#)]
35. Yang, X.; Ma, N.; Yang, L.; Zheng, Y.; Zhen, Z.; Li, Q.; Xie, M.; Li, J.; Zhang, K.Q.; Yang, J. Two Rab GTPases play different roles in conidiation, trap formation, stress resistance, and virulence in the nematode-trapping fungus *Arthrobotrys oligospora*. *Appl. Microbiol. Biotechnol.* **2018**, *102*, 4601–4613. [[CrossRef](#)]
36. Yang, L.; Li, X.; Xie, M.; Bai, N.; Yang, J.; Jiang, K.; Zhang, K.Q.; Yang, J. Pleiotropic roles of Ras GTPases in the nematode-trapping fungus *Arthrobotrys oligospora* identified through multi-omics analyses. *iScience* **2021**, *24*, 102820. [[CrossRef](#)]
37. Yang, L.; Li, X.; Bai, N.; Yang, X.; Zhang, K.Q.; Yang, J. Transcriptomic analysis reveals that Rho GTPases regulate trap development and lifestyle transition of the nematode-trapping fungus *Arthrobotrys oligospora*. *Microbiol. Spectr.* **2022**, *10*, e0175921. [[CrossRef](#)]
38. Chen, Y.; Liu, J.; Fan, Y.; Kang, S.; Wei, D.; Liu, X. SNARE protein DdVam7 of the nematode-trapping fungus *Drechslerella dactyloides* regulates vegetative growth, conidiation, and the predatory process via vacuole assembly. *Microbiol. Spectr.* **2022**, *10*, e0187222. [[CrossRef](#)]
39. Chen, Y.L.; Gao, Y.; Zhang, K.Q.; Zou, C.G. Autophagy is required for trap formation in the nematode-trapping fungus *Arthrobotrys oligospora*. *Environ. Microbiol. Rep.* **2013**, *5*, 511–517. [[CrossRef](#)]
40. Kumar, S.; Stecher, G.; Tamura, K. MEGA7: Molecular evolutionary genetics analysis version 7.0 for Bigger datasets. *Mol. Biol. Evol.* **2016**, *33*, 1870–1874. [[CrossRef](#)]
41. Xie, M.; Wang, Y.; Tang, L.; Yang, L.; Zhou, D.; Li, Q.; Niu, X.; Zhang, K.Q.; Yang, J. AoStuA, an APSES transcription factor, regulates the conidiation, trap formation, stress resistance and pathogenicity of the nematode-trapping fungus *Arthrobotrys oligospora*. *Environ. Microbiol.* **2019**, *21*, 4648–4661. [[CrossRef](#)] [[PubMed](#)]
42. Zhu, M.C.; Zhao, N.; Liu, Y.K.; Li, X.M.; Zhen, Z.Y.; Zheng, Y.Q.; Zhang, K.Q.; Yang, J.K. The cAMP-PKA signalling pathway regulates hyphal growth, conidiation, trap morphogenesis, stress tolerance, and autophagy in *Arthrobotrys oligospora*. *Environ. Microbiol.* **2022**, *24*, 6524–6538. [[CrossRef](#)] [[PubMed](#)]
43. Tunlid, A.; Ahman, J.; Oliver, R.P. Transformation of the nematode-trapping fungus *Arthrobotrys oligospora*. *FEMS Microbiol. Lett.* **1999**, *173*, 111–116. [[CrossRef](#)] [[PubMed](#)]
44. Jiang, K.X.; Liu, Q.Q.; Bai, N.; Zhu, M.C.; Zhang, K.Q.; Yang, J.K. AoSsk1, a response regulator required for mycelial growth and development, stress responses, trap formation, and the secondary metabolism in *Arthrobotrys oligospora*. *J. Fungi* **2022**, *8*, 260. [[CrossRef](#)] [[PubMed](#)]
45. Zhou, D.; Zhu, Y.; Bai, N.; Yang, L.; Xie, M.; Yang, J.; Zhu, M.; Zhang, K.Q.; Yang, J. AoATG5 plays pleiotropic roles in vegetative growth, cell nucleus development, conidiation, and virulence in the nematode-trapping fungus *Arthrobotrys oligospora*. *Sci. China Life Sci.* **2022**, *65*, 412–425. [[CrossRef](#)] [[PubMed](#)]
46. Li, C.; Melesse, M.; Zhang, S.; Hao, C.; Wang, C.; Zhang, H.; Hall, M.C.; Xu, J.R. FgCDC14 regulates cytokinesis, morphogenesis, and pathogenesis in *Fusarium graminearum*. *Mol. Microbiol.* **2015**, *98*, 770–786. [[CrossRef](#)] [[PubMed](#)]
47. Li, X.; Zhu, M.; Liu, Y.; Yang, L.; Yang, J. *Aoatg11* and *Aoatg33* are indispensable for mitophagy, and contribute to conidiation, the stress response, and pathogenicity in the nematode-trapping fungus *Arthrobotrys oligospora*. *Microbiol. Res.* **2023**, *266*, 127252. [[CrossRef](#)]
48. Shoji, J.Y.; Arioka, M.; Kitamoto, K. Vacuolar membrane dynamics in the filamentous fungus *Aspergillus oryzae*. *Eukaryot. Cell* **2006**, *5*, 411–421. [[CrossRef](#)]
49. Xie, M.; Ma, N.; Bai, N.; Yang, L.; Yang, X.; Zhang, K.Q.; Yang, J. PKC-SWI6 signaling regulates asexual development, trap formation, and lifestyle transition in nematode-trapping fungus *Arthrobotrys oligospora*. *Sci. China Life Sci.* **2022**, *65*, 2455–2471. [[CrossRef](#)]
50. He, Z.Q.; Tan, J.L.; Li, N.; Zhang, H.X.; Chen, Y.H.; Wang, L.J.; Zhang, K.Q.; Niu, X.M. Sesquiterpenyl epoxy-cyclohexenoids and their signaling functions in nematode-trapping fungus *Arthrobotrys oligospora*. *J. Agric. Food Chem.* **2019**, *67*, 13061–13072. [[CrossRef](#)]
51. Wei, L.X.; Zhang, H.X.; Tan, J.L.; Chu, Y.S.; Li, N.; Xue, H.X.; Wang, Y.L.; Niu, X.M.; Zhang, Y.; Zhang, K.Q. Arthrobotrisins A-C, oligosporons from the nematode-trapping fungus *Arthrobotrys oligospora*. *J. Nat. Prod.* **2011**, *74*, 1526–1530. [[CrossRef](#)]
52. Zhang, A.X.; Mouhoumed, A.Z.; Tong, S.M.; Ying, S.H.; Feng, M.G. BrlA and AbaA govern virulence-required dimorphic switch, conidiation, and pathogenicity in a fungal insect pathogen. *mSystems* **2019**, *4*, e00140-19. [[CrossRef](#)]
53. Jia, L.; Yu, J.H.; Chen, F.; Chen, W. Characterization of the asexual developmental genes *brlA* and *wetA* in *Monascus ruber* M7. *Fungal Genet. Biol.* **2021**, *151*, 103564. [[CrossRef](#)]
54. Zhang, J.G.; Xu, S.Y.; Ying, S.H.; Feng, M.G. Roles of BrlA and AbaA in mediating asexual and insect pathogenic lifecycles of *Metarhizium robertsii*. *J. Fungi* **2022**, *8*, 1110. [[CrossRef](#)]
55. Li, F.; Shi, H.Q.; Ying, S.H.; Feng, M.G. WetA and VosA are distinct regulators of conidiation capacity, conidial quality, and biological control potential of a fungal insect pathogen. *Appl. Microbiol. Biotechnol.* **2015**, *99*, 10069–10081. [[CrossRef](#)]
56. Etxebeste, O.; Garzia, A.; Espeso, E.A.; Ugalde, U. *Aspergillus nidulans* asexual development: Making the most of cellular modules. *Trends Microbiol.* **2010**, *18*, 569–576. [[CrossRef](#)]
57. Park, H.S.; Yu, J.H. Genetic control of asexual sporulation in filamentous fungi. *Curr. Opin. Microbiol.* **2012**, *15*, 669–677. [[CrossRef](#)]

58. Li, S.; Zhang, S.; Li, B.; Li, H. The SNARE protein CfVam7 is required for growth, endoplasmic reticulum stress response, and pathogenicity of *Colletotrichum fructicola*. *Front. Microbiol.* **2021**, *12*, 736066. [[CrossRef](#)]
59. Dou, X.; Wang, Q.; Qi, Z.; Song, W.; Wang, W.; Guo, M.; Zhang, H.; Zhang, Z.; Wang, P.; Zheng, X. MoVam7, a conserved SNARE involved in vacuole assembly, is required for growth, endocytosis, ROS accumulation, and pathogenesis of *Magnaporthe oryzae*. *PLoS ONE* **2011**, *6*, e16439. [[CrossRef](#)]
60. Lesage, G.; Shapiro, J.; Specht, C.A.; Sdicu, A.M.; Ménard, P.; Hussein, S.; Tong, A.H.; Boone, C.; Bussey, H. An interactional network of genes involved in chitin synthesis in *Saccharomyces cerevisiae*. *BMC Genet.* **2005**, *6*, 8. [[CrossRef](#)]
61. Yang, J.; Zhang, K.Q. Chitin synthesis and degradation in fungi: Biology and enzymes. *Adv. Exp. Med. Biol.* **2019**, *1142*, 153–167. [[PubMed](#)]
62. Goldman, D.L.; Vicencio, A.G. The chitin connection. *mBio* **2012**, *3*, e00056-12. [[CrossRef](#)] [[PubMed](#)]
63. Zhang, H.; Li, B.; Fang, Q.; Li, Y.; Zheng, X.; Zhang, Z. SNARE protein FgVam7 controls growth, asexual and sexual development, and plant infection in *Fusarium graminearum*. *Mol. Plant Pathol.* **2016**, *17*, 108–119. [[CrossRef](#)]
64. Moreau, K.; Ravikumar, B.; Renna, M.; Puri, C.; Rubinsztein, D.C. Autophagosome precursor maturation requires homotypic fusion. *Cell* **2011**, *146*, 303–317. [[CrossRef](#)] [[PubMed](#)]
65. Nair, U.; Klionsky, D.J. Autophagosome biogenesis requires SNAREs. *Autophagy* **2011**, *7*, 1570–1572. [[CrossRef](#)]
66. Davis, S.; Wang, J.; Ferro-Novick, S. Crosstalk between the secretory and autophagy pathways regulates autophagosome formation. *Dev. Cell* **2017**, *41*, 23–32. [[CrossRef](#)]
67. Rajput, S.S.; Chinchwadkar, S.; Aher, A.; Matheshwaran, S.; Manjithaya, R. Exocyst subcomplex functions in autophagosome biogenesis by regulating Atg9 trafficking. *J. Mol. Biol.* **2019**, *431*, 2821–2834.
68. Jones, K.; Kang, C.H. Vacuole dynamics in rice cells invaded by the blast fungus *Magnaporthe oryzae*. *Methods Mol. Biol.* **2018**, *1789*, 195–203.
69. Mochizuki, S.; Minami, E.; Nishizawa, Y. Live-cell imaging of rice cytological changes reveals the importance of host vacuole maintenance for biotrophic invasion by blast fungus, *Magnaporthe oryzae*. *Microbiology* **2015**, *4*, 952–966. [[CrossRef](#)]
70. Tsui, M.M.; Tai, W.C.; Banfield, D.K. Selective formation of Sed5p-containing SNARE complexes is mediated by combinatorial binding interactions. *Mol. Biol. Cell* **2001**, *12*, 521–538. [[CrossRef](#)]
71. Yu, X.; Hu, X.; Pop, M.; Wernet, N.; Kirschhöfer, F.; Brenner-Weiß, G.; Keller, J.; Bunzel, M.; Fischer, R. Fatal attraction of *Caenorhabditis elegans* to predatory fungi through 6-methyl-salicylic acid. *Nat. Commun.* **2021**, *12*, 5462. [[CrossRef](#)]
72. Yang, J.; Wang, W.; Liu, Y.; Xie, M.; Yang, J. The MADS-box transcription factor AoRlmA is involved in the regulation of mycelium development, conidiation, cell-wall integrity, stress response, and trap formation of *Arthrobotrys oligospora*. *Microbiol. Res.* **2023**, *268*, 127299. [[CrossRef](#)]

Disclaimer/Publisher’s Note: The statements, opinions and data contained in all publications are solely those of the individual author(s) and contributor(s) and not of MDPI and/or the editor(s). MDPI and/or the editor(s) disclaim responsibility for any injury to people or property resulting from any ideas, methods, instructions or products referred to in the content.